The chemical process of producing activated carbon using walnut shells and plastic wastes

Hosein Bazgir[1] · Mohammad Reza Rostami[1] · Salar Tavakkol[2] · Zahra Issaabadi[1] · Hamed Mohamadzadeh Shirazi[3] · Bahman Goshayeshi[3] · Kevin M. Van Geem[3] · Mehdi Nekoomanesh Haghighi[1] · Mehrdad Seifali Abbas-Abadi[1,3]

Abstract

In this work, the chemical preparation of activated carbon (*AC*) using walnut shell (*WS*) and plastic wastes (primarily consist-ing of polyethylene, polypropylene, and polystyrene) as feedstocks and chemical activators (KOH and NaOH) was investi-gated in a fixed-bed reactor. Thermogravimetric analysis (TG) (TGA) was used to carbonize *WS* together with plastic waste. Furthermore, the Brunauer–Emmett–Teller (BET) method, FTIR, dye adsorption, iodine number, and SEM experiments were applied to characterize the obtained *AC*s. The results indicated that the polyolefinic waste acted as insulation and controlled the energy reaching *WS* particles to a certain extent. In addition, the reactive pyrolysis products of plastics such as styrene and light olefins reacted with the unstable structure of *WS* and intensified the secondary reactions during the carbonization process. Secondary reactions led to the creation of new structures that were clearly visible in the FTIR spectra. Also, the results indicated that the participation of plastics in secondary reactions has led to an increase in *AC* production. Furthermore, during the activation process, plastics have led to a significant increase in the surface area and volume of pores. The curve of *WS* degradation together with plastic waste showed that plastics have slowed down the *WS* degradation, as indicated by the slope of the degradation graph has clearly decreased.

✉ Kevin M. Van Geem
Kevin.VanGeem@UGent.be

✉ Mehdi Nekoomanesh Haghighi
M.Nekoomanesh@IPPI.ac.ir

✉ Mehrdad Seifali Abbas-Abadi
Mehrdad.Seifali@ugent.be

[1] Polymerization Engineering, Iran Polymer and Petrochemical Institute (IPPI), P.O. Box 14965/115, Tehran, Iran

[2] Institute for Technical Chemistry, Karlsruhe Institute of Technology, Karlsruhe, Germany

[3] Laboratory for Chemical Technology, Department of Materials, Textiles and Chemical Engineering, Faculty of Engineering & Architecture, Ghent University, Technologiepark 125, B-9052 Zwijnaarde, Belgium

Graphical abstract

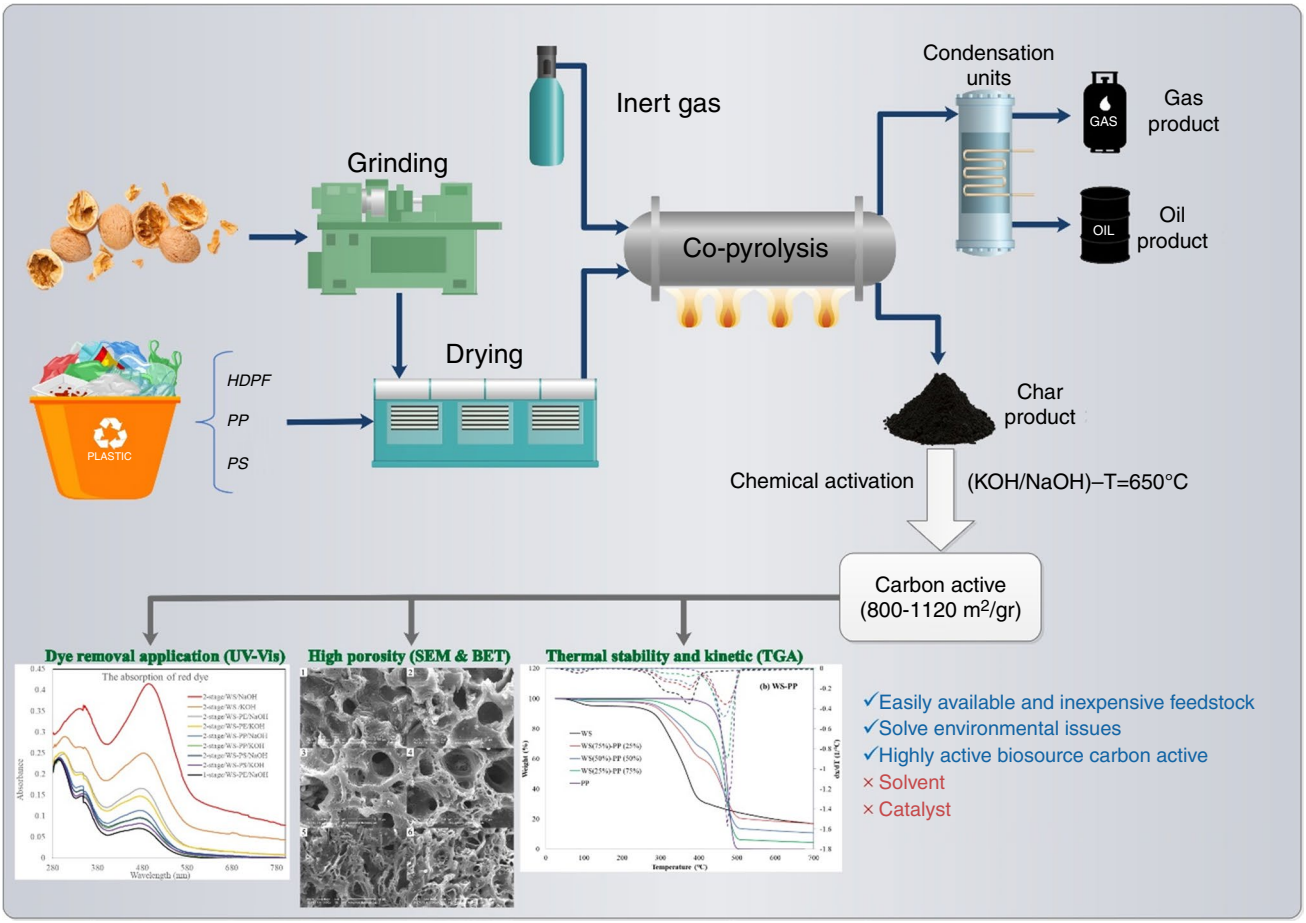

Keywords Walnut shell · Plastic waste · Activated carbon · Pyrolysis · TG

Introduction

For years, activated carbon (*AC*) has been used in different chemical industries for various applications, e.g., water and wastewater treatment, water desalination, chemicals treatment, and air purification [1–3]. As a porous substance with a high surface area, *AC* can be applied as a strong physical adsorbent. *AC* is mainly composed of carbon (> 90%) with a polyaromatic structure [4]. Other elements that are mainly found in *AC* include oxygen, hydrogen, nitrogen, and sulfur mostly as functional groups [5].

Annually, more than one hundred thousand tons of *AC* are produced all over the world [6]. Mainly wood, coconut shell, bitumen charcoal, peat shell, anthracite, lignite olive, and almond shell are used as feedstock [7]. Maintaining strength and physical structure under various mechanical and thermal stresses is one of the key parameters of *AC* granular type and results in greater efficiency during the *AC* application [8]. Activation treatment of *AC* is performed in two physical and chemical procedures [9]. The physical method is usually performed in two stages. The first stage includes pyrolysis and carbonization in a neutral media and physical activation in the second stage in an oxidizing atmosphere, e.g., steam and CO_2 in the temperature range of 800–1100 °C [2, 10, 11]. Furthermore, *AC* can be produced in single-stage under an oxidizer atmosphere from the beginning [12]. In chemical activation as wet oxidation, feedstock or carbonized feedstock is impregnated with a chemical agent and activated at a temperature range (400–900 ℃) usually lower than the physical method [13]. In the activation process, the activating agent mainly reacts with the

weak structures in *AC,* e.g., defective polyaromatics, and some functional groups leading to the intensification of pores formation in the *AC* bulk [14]. Furthermore, the reaction of the activating agent with functional groups in activated carbon results in new functional groups, and many of the previous functional groups are also neutralized [12].

Varied acid, base, and salt activators, e.g., phosphoric acid (H_3PO_4) [15], sulfuric acid (H_2SO_4) [16], zinc chloride ($ZnCl_2$) [17], potassium carbonate (K_2CO_3) [18], sodium hydroxide (NaOH) [19], and potassium hydroxide (KOH) [20] react with degradable parts of feedstock (before and/or after carbonization). In addition to increasing the activation rate, activators by creating different functional groups on the surface of *AC*, can determine the *AC* efficiency and application to some extent [21]. In recent years, KOH has been widely used in the production of low-cost *AC*. Among the various activators, KOH has been extensively used, due to its ability to produce *AC* with a high surface area, narrow distribution of pore size, low environmental pollution, less corrosiveness, and lower cost [22].

Degradation and carbonization mechanisms during the pyrolysis and activation process play a significant role in the physical and mechanical properties of the prepared matrix [23, 24]. *AC* with a high surface area and porous structure, if it is not accompanied by high mechanical strength, will quickly collapse and lose its effectiveness [25, 26]. The intensification of secondary reactions such as Diels–Alder, repolymerization, and cross-linking, which are effective in the formation of aromatics and polyaromatics, can reduce structural defects and resist mechanical and thermal stresses [27, 28]. Slow pyrolysis by intensifying secondary reactions can play an effective role in the production of quality activated carbons [29]. Consequently, the TG instrument applied to evaluate the degradation mechanisms can play an effective role in studying the production process of *AC* [30].

The co-pyrolysis of plastics with different materials has been repeatedly evaluated in different fields [31–33], but so far it has not been investigated in the field of *AC* production. Since plastics can affect the process of biomass degradation [31], hence, in this paper, it has been tried to study this process in a laboratory reactor and TG instrument.

In this paper, an attempt has been made to investigate the effect of plastic wastes, e.g., polyethylene (PE), polypropylene (PP), and polystyrene (PS) on the production of *AC* from *WS*. The chemical activation process using KOH/NaOH has been carried out in a two-stage and one-stage using a fixed-bed reactor. To check the results more closely and study the degradation mechanisms, the co-pyrolysis process using TG instrument has also been investigated. Furthermore, the *AC*s produced have been evaluated using BET method, SEM, dye adsorption, iodine number, and FTIR experiments.

Materials and methods

Materials

WS was prepared from an Iranian walnut type available in the market and was powdered using a laboratory mill in the size of 150–200 microns. Plastic wastes without minerals and masterbatch including PP, PE, and PS were obtained from household waste and were milled in the size of 150–500 microns. Nitrogen (purity 99.9%) gas was supplied by Roham Co (Tehran, Iran). KOH, NaOH, and HCl were purchased from Merck.

Instruments and methods

BET method

Brunauer–Emmett–Teller (BET) method (Quantachrome Corp. Nova 2200, Version 7) was applied to determine textural properties of prepared *AC*s in terms of BET surface area (*SA*) and total pore volume (*TPV*) by nitrogen adsorption at − 196 ℃.

Ash measurement

To measure the ash content, 2 g of each sample was placed in a quartz boat. The samples were kept in a muffle furnace at 900 ℃ for 2 h and then cooled to room temperature and weighed. According to the following formula, the ratio of the remaining ash to the sample (2 g) was calculated as the ash content (%).

$$\text{Ash Content } (\%) = 100 \times \text{ash}(g)/2g \quad (1)$$

Elemental analysis

The elemental composition of *WS* and plastic wastes was analyzed by the CHNS Vario EL III Elemental Analyzer.

Higher heating value

The higher heating value (*HHV*) of different feedstocks was measured using an isoperibol bomb calorimeter (Parr 1261; Parr Instrument Company, USA).

SEM

The morphology of prepared *AC*s was observed by scanning electron microscopy (SEM model S-3000 N, Hitachi, Japan)

after being coated by a gold sputtering machine (model E-1010, Hitachi, Japan). The magnification of the SEM was selected as × 3 K in this study.

FTIR

The FTIR spectrum of samples was recorded using a Model Perkin Elmer 1100 series FTIR operating in the range 4000–400 cm^{-1} by using KBr crystals to prepare the pellet.

Iodine number

The iodine number of samples was determined by the sodium thiosulfate volumetric method. A certain amount of *AC* (0.5 g) was added into 10 mL of 5% (v/v) HCl solution. To remove the sulfur content, the solution was gently boiled for 30 s and then cooled to room temperature. Subsequently, 50 mL of standardized iodine solution with 0.1 M concentration was added and stirred for 15–20 min and filtered quickly. The remaining filtrate was titrated by sodium thiosulfate ($Na_2S_2O_3$) standardized solution and starch solution as indicator.

Dye adsorption

The dye adsorption capability of the prepared *AC*s was considered by the spectrophotometer method. A solution of Congo red and acid yellow 23 dyes (600 $mg{\cdot}L^{-1}$) was prepared, and 0.1 g of *AC*s was added in a 100-mL glass conical beaker and shaken for 2 h at room temperature to reach equilibrium. The adsorbent was separated by centrifugation at 5000 rpm for 15 min, and 2 cc of the solution was withdrawn and analyzed by 722 Raster Spectrophotometer (UV-2450, Shimadzu, Japan).

Thermogravimetric analysis (TG)

TG instrument (model Netzsch TG 209) was applied to study the thermal behavior of *WS* and plastic wastes (PE, PP, and PS) under the heating rate of 30 ℃·min^{-1} at 30–700 ℃. In order to minimize the test error, the mass of all the samples was equal to 12 mg. TG experiments were performed in nitrogen media (99.99% minimum purity) at a flow rate of 30 $mL{\cdot}min^{-1}$.

In DTG curves, T_1^{peak} and T_2^{peak} are the temperatures at which the maximum degradation rates of *WS* and plastic occur, respectively. Furthermore, α_1 and α_2 are the slopes of degradation curves of *WS*' cellulose and hemicellulose, and plastic respectively, while α_3 represents the slope of degradation curves of biochar and char for *WS* and plastics, respectively.

The fixed-bed reactor

The *AC* production was carried out in two single-stage and two-stage methods. The reactor used was a small laboratory fixed-bed reactor with a capacity of 100 cc and a heating rate of around 10 ℃·min^{-1} (Fig. 1). The reactor's temperature and pressure were controlled. In the single-stage method, *WS* with a plastic waste was mixed physically in different ratios, immersed into water solutions of NaOH or KOH and held in the solutions for 24 h, heated in the pyrolysis reactor in a nitrogen media, and placed at a temperature of 650 ℃ for 30 min. In the two-stage process, *WS* and plastic were added to the pyrolysis reactor in different ratios and placed under nitrogen gas for 30 min at a temperature of 500 ℃. In the following, after cooling down, the obtained charcoal was immersed into water solutions of NaOH or KOH and held in the solutions for 24 h, and the activation process was performed at 650 ℃ under a nitrogen atmosphere for 30 min.

To evaluate the process efficiency, in two-staged method, as mentioned in Eqs. 2–4, Y_1 and Y_2 represent the mass percentage of the remaining charcoal per the total mass of the sample and the of *WS* in the sample, respectively, while Y_3 was applied to measure the percentage of the remaining *AC* per the of charcoal.

$$Y_1(\text{mass}/\%) = 100 \times \text{charcoal}\ (g)/(\text{WS}(g) + \text{Plastic}\ (g)) \tag{2}$$

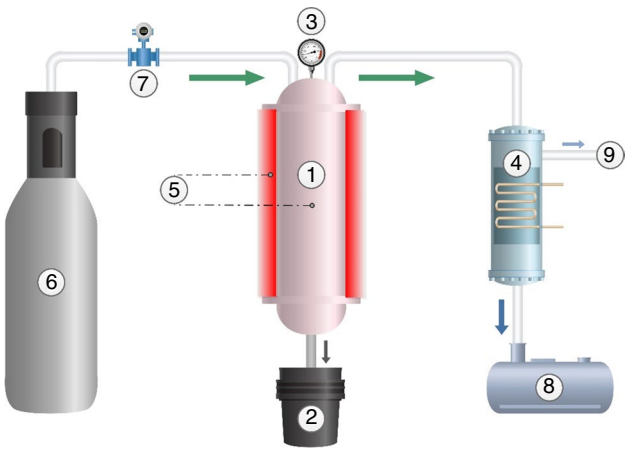

Fig. 1 The activation pilot plant: (1) pyrolysis reactor, (2) char storage, (3) pressure gauge, (4) condensate columns, (5) thermocouple, (6) nitrogen bottle, (7) nitrogen flow meter, (8) liquid storage, and (9) vent

$$Y_2(\text{mass}/\%) = 100 \times \text{charcoal}\ (g)/ \\ (\text{only WS}(g)\ \text{share of the feedstock}) \quad (3)$$

$$Y_3(\text{mass}/\%) = 100 \times \text{AC}(g)/(\text{charcoal}\ (g)) \quad (4)$$

And for single-staged method:

$$Y_1'(\text{mass}/\%) = 100 \times \text{AC}(g)/(\text{WS}(g) + \text{Plastic}\ (g)) \quad (5)$$

$$Y_2'(\text{mass}/\%) = 100 \times \text{AC}(g)/(\text{only WS}(g)\ \text{share of the feedstock}) \quad (6)$$

Results and discussion

The results of CHNS analysis, ash, and *HHV* of *WS* along with the plastic wastes are given in Table 1. In the used *WS*, carbon, hydrogen, nitrogen, and oxygen content were 44.9, 4.9, 0.3, and 48.3%, respectively, while PE, PP, and PS contained hydrogen and carbon, and oxygen accounted for a small share of plastics (< 0.1%). The hydrogen content in PE, PP, and PS was 14.3, 8.0, and 14.5%, respectively. The presence of aromatics in the PS structure results in a considerable reduction of hydrogen than polyolefins. Due to the usage of pure plastic wastes, the remaining ash from burning was negligible, while the remaining ash from the burning of *WS* due to minerals was around 1.6%. Furthermore, due to the high oxygen and nitrogen content in the *WS* structure, like other biomass [34], and the lack of participation in heat generation, *WS* resulted significantly in less *HHV* (15.3 kJ·kg^{-1}) than plastics (PE: 44.2 kJ·kg^{-1}, PP: 43.8 kJ·kg^{-1}, and PS: 40.5 kJ·kg^{-1}) [35]. Furthermore, polyolefins showed slightly more *HHV* than PS regarding hydrogen content.

The two-stage-activated carbon preparation process

Table 2 indicates the results of quantitative and qualitative analysis of the produced *AC*s in a two-stage process. In the pyrolysis stage, 20 g of the mixture of a plastic (0, 25%) and *WS* (100, 75%) was placed in a fixed-bed reactor. The complex and layered structure of *WS* with high oxygen content, which lead to double bonds and radicals during deoxygenation, provides a suitable environment for secondary reactions, e.g., repolymerization, cross-linking, Diels–Alder, and carbonization reactions [36]. During slow pyrolysis of biomass, intensification of secondary chain reactions, along with the aromatic-based structure of lignin, result in more charcoal formation [37, 38]. Hence, the residual charcoal can be a determinative parameter to study the impact of primary and secondary reactions in biomass pyrolysis. As can be seen in Table 2 (Y_1), the efficiency of the remaining charcoal from the pyrolysis of *WS* was slightly higher than the co-pyrolysis of plastics and *WS* (37.0–34.2%). Given that plastics leave negligible coke, it was expected that the efficiency of residual charcoal would not differ significantly with respect to the *WS* content of the samples (Y_2), while residual charcoal increased significantly in the presence of plastic (37.0–47.3%), indicating obvious transactions and impact of the applied plastics on *WS* during the co-pyrolysis. The results show that the participation of plastic has led to the intensification of secondary reactions in the direction of carbonization and the formation of new aromatic structures.

In the following, the obtained charcoal (3 g) was physically mixed with KOH and NaOH activators in a ratio of 3–1. What can be concluded from the results was that new structures have been generated during the co-pyrolysis of plastics and *WS*, which have a different specification than normal biochar and show a different response to activation by chemicals. New polyaromatic structures are hydrocarbon-based regarding the used plastic types. Due to the absence of heterogeneous atoms such as oxygen, they have lower defects and higher thermal stability. Furthermore, by generating new layers on the biochar surface, it can be effective in increasing the surface area. In the activation process, the activators were faced with a biochar that has relatively experienced a stronger carbonization process during the co-pyrolysis process and has less structural defects. Hence, even in the spots that face intense activation and the walls become very thin, due to the high mechanical strength, it does not collapse and resulting in a highly porous *AC* with a high surface area. The results indicate that the utilization of KOH, in contrast to NaOH, has led to an increase in the amount of

Table 1 The elemental composition, ash and *HHV* of the used raw materials

Sample	Elements				Ash/%	*HHV*/kJ·kg^{-1}
	Carbon/%	Hydrogen/%	Nitrogen/%	Oxygen*/%		
WS	44.9	4.9	0.3	48.3	1.6	15.3
PE	85.6	14.3	0.0	0.1	0.0	44.2
PS	91.9	8.0	0.0	0.1	0.0	40.5
PP	85.4	14.5	0.0	0.1	0.0	43.8

*Determined by difference

Table 2 Effect of PE, PP, and PS on the prepared AC by chemical activation using the two-stage process

No	Pyrolysis				Activation				SA^1 /$m^2 \cdot g^{-1}$	TPV^2 /$m^2 \cdot g^{-1}$	$V_{micro}{}^3$ /$m^3 \cdot g^{-1}$	$V_{meso}{}^4$ /$m^3 \cdot g^{-1}$	Iodine number /$mg \cdot g^{-1}$
	WS/%	PE/%	PP/%	PS/%	Y_1/%	Y_2/%	Char/%	NaOH/%	KOH/%	Y_3/%				
1	100	0	0	0	37	37	75	25	0	54.2	810	0.54	0.09	0.42	760
2								0	25	50.8	833	0.59	0.16	0.41	782
3	75	25	0	0	34.2	45.6	75	25	0	63.7	855	0.62	0.13	0.46	805
4								0	25	60.8	870	0.63	0.15	0.46	821
5	75	0	25	0	34.7	46.3	75	25	0	66.9	891	0.62	0.18	0.41	803
6								0	25	62.5	937	0.64	0.18	0.44	852
7	75	0	0	25	35.5	47.3	75	25	0	67.2	1146	0.72	0.21	0.45	1101
8								0	25	65.6	1194	0.76	0.25	0.47	1150

[a]BET surface area; [b]Total pore volume; [c]Micropore volume; [d]Mesopore volume

surface area and pores generated in the activated carbons. The reason behind this could be that activation with KOH could create an increased number of micropores, resulting in a higher volume of micropores and consequently leading to the formation of porous carbon with a larger surface area which is in line with similar studies [39]. Moreover, the results indicate that at charcoals modified with plastics, more *TPV* (0.54–0.76 $m^3 \cdot g^{-1}$) and BET surface area (810–1194 $m^2 \cdot g^{-1}$) have been generated than the typical charcoal. Furthermore, the findings indicate that the utilization of NaOH and KOH activators predominantly yields micro- (0.09–0.16 $m^3 \cdot g^{-1}$) and mesopores (0.41–0.42 $m^3 \cdot g^{-1}$). Additionally, the utilization of waste plastics generates more micropores (0.09–0.25 $m^3 \cdot g^{-1}$) (Table 2). The secondary reactions resulting from the co-pyrolysis of waste plastics and *WS* with forming new surfaces results in the creation of more micropores.

In the comparison between plastics, PS has shown superior performance over polyolefins in increasing BET surface area (1194–855 $m^2 \cdot g^{-1}$) and *TPV* (0.76–0.62 $m^3 \cdot g^{-1}$). The lower temperature of PS degradation and greater participation in the degradation of cellulose and hemicellulose, along with the greater activity of styrene in Diels–Alder reactions can result in more efficiency of PS during the co-pyrolysis process. In the following, the iodine number was applied to determine the adsorption efficiency of activated carbons. As can be seen, with the increase in porosity and surface area, the iodine absorption has increased (760–1150 $mg \cdot g^{-1}$) and the mixture of PS and *WS* has led to the highest iodine number in the used feedstocks. Furthermore, in the comparison between the used activators, KOH showed somewhat a better performance in terms of *TPV* (0.59–0.54 $m^3 \cdot g^{-1}$) and BET surface area (833–810 $m^2 \cdot g^{-1}$) compared to NaOH.

The single-stage-activated carbon preparation process

In the single-stage activation process, the mixture of *WS* and plastics along with the activator was placed in the reactor simultaneously. As shown in Table 3, like the two-stage method, the results indicated that KOH showed a better activation performance than NaOH which led to more BET surface area (983–901 $m^2 \cdot g^{-1}$) and *TPV* (0.80–0.74 $m^3 \cdot g^{-1}$). Also, another noteworthy point, using NaOH activator, the yield of the produced *AC* by the mixtures was higher than that of pure *WS* (Y'_1: 15.3–23.5%). Considering that 25% of the feedstock was made up of plastics, the yield of *AC* produced in the single-stage activation process has increased significantly with respect to the *WS* content (Y'_2: 15.3–31.3%). Furthermore, similar to the two-stage process, plastics have significantly increased the created structures during the activation process. The increase in *TPV* (0.64–0.79 $m^3 \cdot g^{-1}$) and BET surface area (901–1262

Table 3 Effect of PE, PP, and PS on the prepared *AC* by chemical activation using the direct process

No	*WS*/%	PE/%	PP/%	PS/%	NaOH/%	KOH/%	Y'_1/%	*Y'2*/%	*SA* /$m^2 \cdot g^{-1}$	*TPV* /$m^3 \cdot g^{-1}$	V_{micro} /$m^3 \cdot g^{-1}$	V_{meso} /$m^3 \cdot g^{-1}$	Iodine number /$mg \cdot g^{-1}$
9	100	0	0	0	100	0	15.3	15.3	901	0.64	0.12	0.51	850
10	100	0	0	0	0	100	14.9	14.9	983	0.68	0.16	0.51	936
11	75	25	0	0	100	0	19.8	26.4	1123	0.74	0.20	0.52	1082
12	75	0	25	0	100	0	21.3	28.4	1110	0.75	0.19	0.54	1061
13	75	0	0	25	100	0	23.5	31.3	1262	0.79	0.21	0.56	1125

$m^2 \cdot g^{-1}$) of *AC* obtained from the mixture was clearly evident compared to *WS*. The obtained results show that the use of waste plastics in a single-stage process increases the volume of micro- (0.12–0.21 $m^3 \cdot g^{-1}$) and mesopores (0.51–0.56 $m^3 \cdot g^{-1}$). The polyaromatic surfaces created by the co-pyrolysis process on the charcoal surface have a uniform structure that exhibit a higher inclination toward forming micropores, as clearly visible in the SEM figures (Fig. 3). The activator reaction with charcoal with high oxygen percentage leads to a porous structure. In the *AC* obtained from the mixture of plastic and *WS*, the iodine absorption (850–1125 $mg \cdot g^{-1}$) was significantly higher than pure *WS* due to the higher surface area and porosity.

The characterization of the produced activated carbons

Figure 2 compares the FTIR spectra of various *AC*s obtained from the single- or two-stage process of *WS* and its mixture with PE, PP, and PS. The *AC* spectrum of pure *WS* is different from the samples obtained from the mixtures. The strong absorption peak at 1437–1442 cm^{-1} corresponds to unsaturated aromatic bonds (C = C ring stretching) which indicates the creation of strong polyaromatic structures on the surface of *WS* biochar [40, 41]. This peak, which is not seen in the *AC* obtained from pure *WS*, indicates the structural difference of the *AC* obtained from the mixture of *WS* and plastic compared to pure *AC*. The broad absorption peak at 3426–3443 cm^{-1} is related to the stretching vibration of hydroxyl (OH) group [40–42]. Furthermore, the characteristic peak of the hydroxyl group of single-stage pyrolysis products is lower than the others. This result can be due to the increase in interaction between the sodium hydroxide and hydroxyl group during the pyrolysis process. The vibration of methine group (CH) also has a peak at 880 cm^{-1} [41, 42]. The small peaks at 1650–1780 cm^{-1} and 2505–2515 cm^{-1} correspond to the stretching of carbonyl (C = O) and thiol (SH) groups, respectively.

Figure 3 shows the SEM of some produced *AC*s. As can be seen, the impact of plastics on products is evident in both single-stage and two-stage methods. In the samples produced

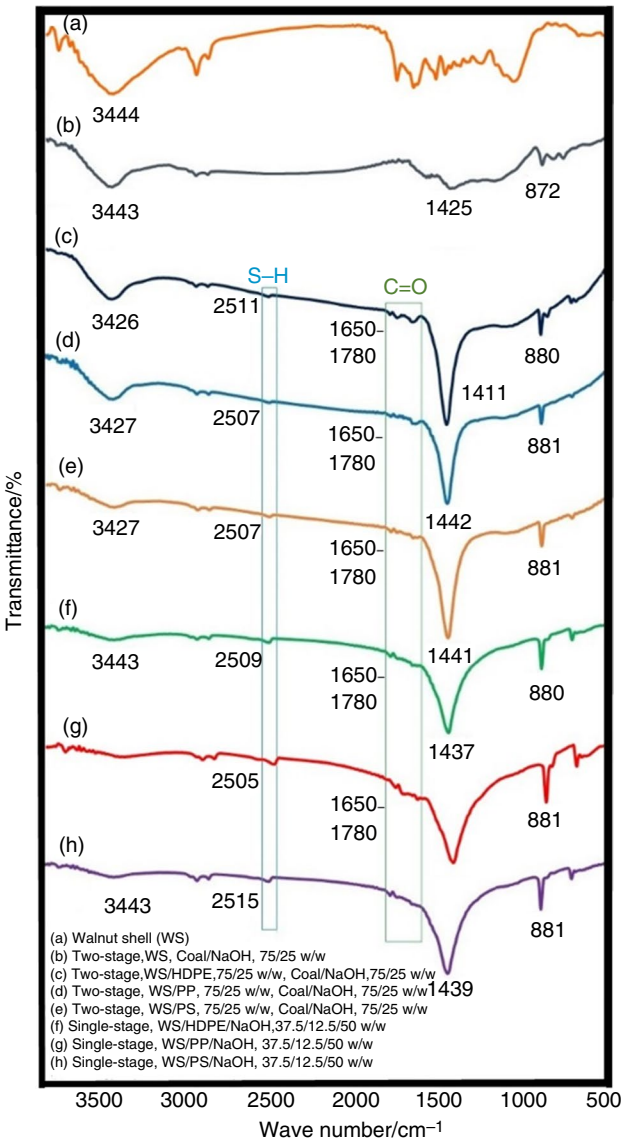

Fig. 2 FTIR spectra of the produced *AC*s

from pure *WS*, mainly large pores are seen. While in the *AC*s produced from a mixture of plastic and *WS*, in the two-stage method, a combination of large and small pores, and in the single-stage method, small pores can be seen. The results

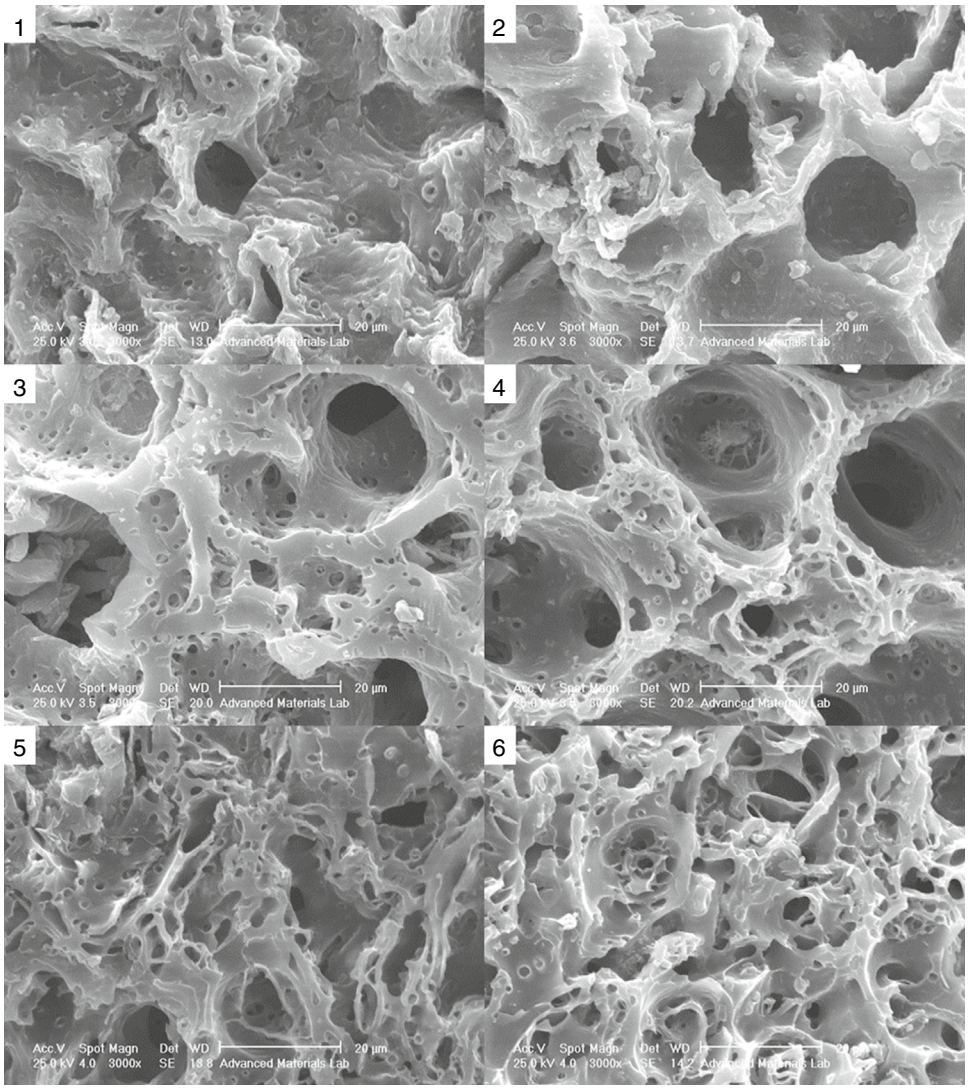

Fig. 3 The SEM micrographs of *AC*s: (1) two-stage/*WS*/NaOH, (2) two-stage/*WS*/KOH, (3) two-stage/*WS*-PS/NaOH, (4) single-stage/*WS*/NaOH, (5) single-stage/*WS*-PE/NaOH, and (6) single-stage/*WS*-PP/NaOH

show that by using plastics in the production process of *AC*, it is possible to control the size of porosity to some extent.

Congo red and acid yellow 23 dyes were used as the dyes found in industrial effluents in order to investigate the performance of the synthesized *AC*s adsorbent. The red dye in the UV test has two main peaks in the region of 300–500 nm. As it is clear from the graphs, using high surface area *AC*s, the peak intensity was decreased clearly. The yellow dye in the UV test has two peaks in the ranges of 280–400 and 500–600 nm, and the intensity of these peaks indicates the remaining concentration of the dye (Fig. 4).

TG study of *WS* and plastic wastes

To better understand the impact of plastics on the carbonization process of *WS*, the degradation process of *WS* degradation was investigated along with polyolefins using TG instrument. The degradation diagram of the *WS* mixture with PE, PP, and PS in different percentages (0, 25, 50, 75, and 100) using a TG instrument is shown in Fig. 5. Furthermore, Table 4 provides kinetic information along with the degradation slope of different sections in the pyrolysis process of the studied mixtures.

As expected [43, 44], PE has completely degraded in a narrow and high-temperature range (T_2^{peak}: 493 ℃). Furthermore, the linear degradation with a steep slope (α_2: 2.349%·℃$^{-1}$) indicates a uniform structure of PE with similar bonds (Fig. 5a), whereas *WS* like other biomasses has lost its in three stages. The water evaporation occupied a small peak in all samples containing *WS* and considering that the process was carried out at atmospheric pressure, it happened around 100 ℃. The degradable structure of hemicellulose and cellulose led to two overlapped peaks during degradation (T_1^{peak}: 374 ℃), while the aromatic-base structure of lignin is highly favorable to Diels–Alder reactions

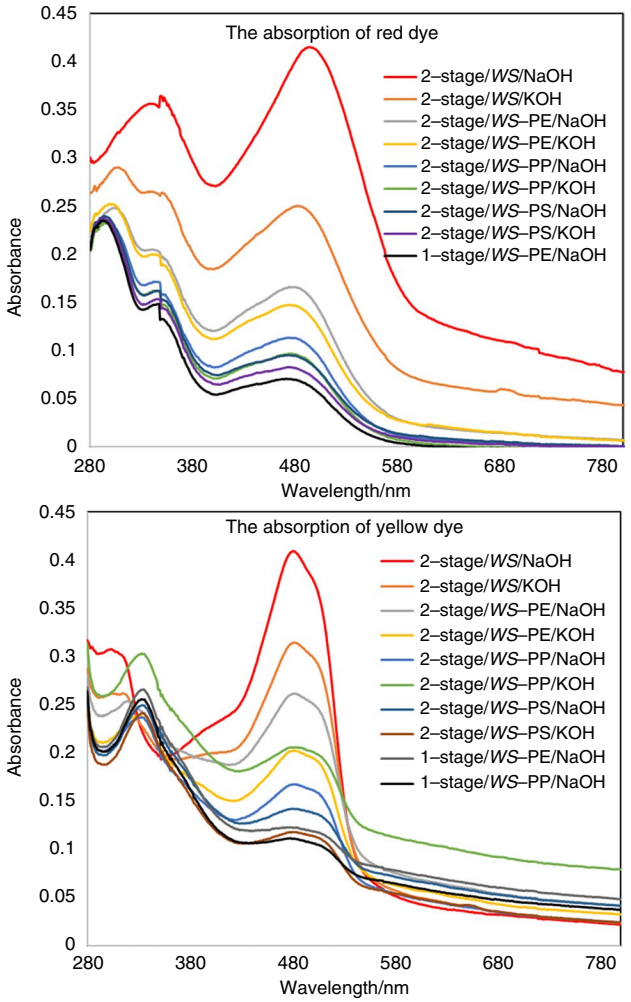

Fig. 4 Absorption spectroscopy of the *AC*s containing Congo red and acid yellow 23 dyes

and the formation of polyaromatics. Hence, lignin lost a small share of its mass at a slow rate (α_3: 0.045% ℃$^{-1}$), and the remaining share left a polyaromatic structure in the reaction with other remaining molecules of cellulose and hemicellulose [45, 46]. The presence of hydroxyl groups in the structure of all three components of biomass is very effective in intensifying deoxygenation reactions leading to water production [47]. By increasing the PE share in the feedstock, the intensity of WS degradation was decreased ($-\mathrm{d}x/\mathrm{d}T_1^{peak}$: 0.35–0.08%·℃$^{-1}$), while stronger PE degradation peak ($-\mathrm{d}x/\mathrm{d}T_2^{peak}$: 0.36–1.57%·℃$^{-1}$) in the DTG curve was seen clearly. For the mixture of *WS* and PE at temperatures less than 400 ℃, as mentioned previously, cellulose and hemicellulose degraded, which can be seen in a separate peak. With the increase in PE share in the feedstock, more molten plastic surrounded the *WS* particles and as a thermal insulant decreased the heating intensity to *WS* particles which resulted in slower *WS* pyrolysis.

Figure 5b shows the degradation diagram of feedstocks containing different shares of PP and *WS* (0, 25, 50, 75, and 100%). As can be seen, PP was degraded in a narrow and lower temperature range (T_2^{peak}: 474 vs. 493 ℃) and with a steeper slope (α_2: 2.564 vs. 2.349%·℃$^{-1}$) than PE regarding the lower activation energy and less tendency to secondary reactions due to more steric hindrance. The results indicated that with increasing PP content in the feedstock, the peak intensity of *WS* degradation ($-\mathrm{d}x/\mathrm{d}T_1^{peak}$: 0.35–0.08%·℃$^{-1}$) was decreased while the intensity of PP degradation peak ($-\mathrm{d}x/\mathrm{d}T_2^{peak}$: 0.36–1.57%·℃$^{-1}$) was increased clearly.

Like polyolefins, PS degraded in a narrow temperature range and at a high rate (α_2: 2.283%·℃$^{-1}$) due to its uniform structure. Furthermore, due to the lower activation energy and lower thermal stability, PS lost its mass in the TG experiment in the lower temperature range (T_2^{peak}: 434 ℃) than polyolefins (Fig. 5 c). The main difference between the co-pyrolysis of PS and *WS* compared to polyolefins is that due to the degradation of PS at lower temperatures, a significant share of PS was degraded along with cellulose and hemicellulose. The simultaneity of degradation increases the possibility of secondary reactions, and hence, as can be seen, the thermal stability of both *WS* (α_1: 0.539–0.140%·℃$^{-1}$) and PS (α_2: 2.283–0.862%·℃$^{-1}$) parts increased significantly compared to the co-pyrolysis of polyolefins and *WS*. The simultaneous degradation of PS with cellulose and hemicellulose and the participation of styrene in secondary reactions led to the creation of new and significant structures on *WS* particles. This process led to a decrease in the degradation rate of the remaining structure from *WS* and PS co-pyrolysis (α_3: 0.045–0.013%·℃$^{-1}$). Hence, the lower degradation rate of the sample containing 25% PS than *WS*, resulted in more remaining charcoal at a temperature of 610 ℃ and higher. The decrease in the graph slope of degradation during co-pyrolysis has been seen in other papers but has not been discussed extensively [48, 49].

Discussion

First of all, it should be considered that most of the biomass that is used for the production of activated carbon usually has a high oxygen content and the deoxygenation process plays a significant role in the activation process and porosity generation [50]. Furthermore, the deoxygenation process leads to the creation of radicals and double bonds, which play an effective role in secondary reactions and carbonization. Moreover, the activators react more with oxygenated functional groups and create more porosity [51]. In addition, to investigate the effect of plastics on *AC* production, different parameters should be considered. One of the most important effects of using plastics is the melting of plastics during the co-pyrolysis process. The melting of plastics causes a

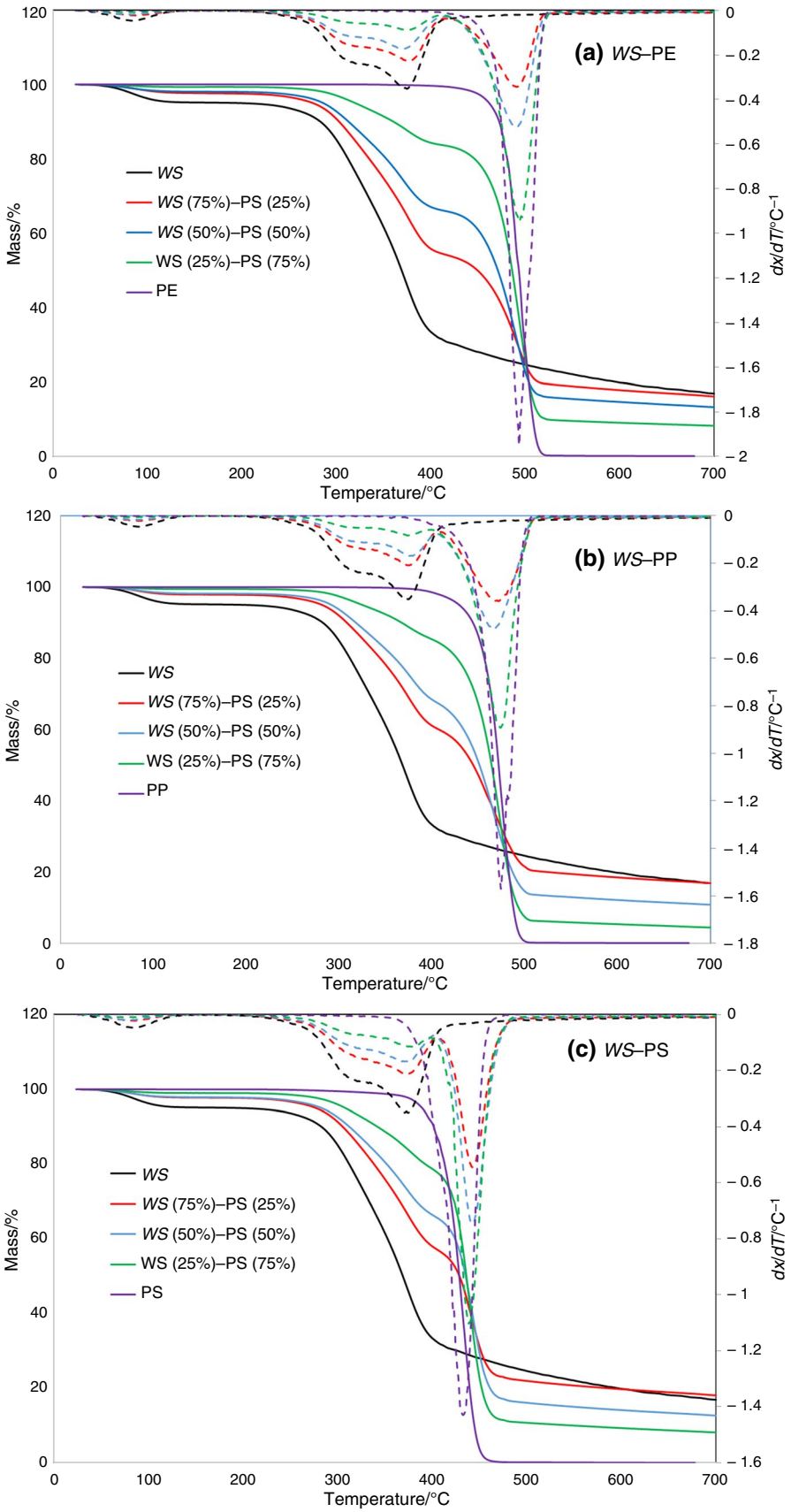

Fig. 5 TG curve and DTG curves of the different blends of **a** PE/*WS*; **b** PP/*WS*; and **c** PS/*WS*

Table 4 Effect of plastic content (%) in the plastic: *WS* blend on the kinetic parameters and characteristic temperatures

Plastic	Plastic/%	Cellulose and hemicellulose			Plastic			Lignin	
		T_1^{peak}/℃	α_1[1]/%·℃$^{-1}$	R^2	T_2^{peak}/℃	α_2/%·℃$^{-1}$	R	α_3/%·℃$^{-1}$	R
PE	0	370	0.539	0.994	–	–	–	0.045	0.971
	25	371	0.358	0.995	492	0.576	0.993	0.018	0.997
	50	373	0.274	0.993	491	0.851	0.990	0.015	0.999
	75	375	0.149	0.997	494	1.369	0.981	0.009	0.997
	100	–	–	–	493	2.349	0.985	0.0007	1
PP	25	372	0.314	0.992	468	0.912	0.990	0.017	0.996
	50	374	0.256	0.993	471	1.224	0.993	0.014	0.999
	75	376	0.172	0.990	474	1.969	0.996	0.010	0.998
	100	–	–	–	474	2.564	0.997	0.0006	0.997
PS	25	373	0.331	0.990	444	0.862	0.991	0.019	0.986
	50	375	0.259	0.991	442	1.154	0.988	0.017	0.998
	75	377	0.170	0.989	438	1.754	0.989	0.013	0.999
	100	–	–	–	434	2.283	0.988	0.0007	0.998

[a]Slope; [2]Correlation coefficient

layer of molten plastic to surround the *WS* particles. Due to the low thermal conductivity and high heat capacity of the plastic, the *WS* particles received less heat, and actually, the *WS* particles experienced a lower heating rate than what was going on in the reactor [31]. On the other hand, lower heating rates result in lower chain scission over cross-link ratio and more carbonization [45]. Furthermore, the molten polymer penetrates into the pores of *WS* particles and somehow reduces the surface of particles to a significant extent, which is also effective in reaching less heat to *WS* particles. Reducing the heating rate in *WS* pyrolysis leads to the intensification of secondary reactions and stronger aromatic structures, especially in the surface walls. The next point that should be considered is the simultaneity of the co-pyrolysis reaction of the polymer with the degradable parts of *WS* in some areas. Styrene, olefins, and diolefins obtained from plastic pyrolysis can easily react with radicals and double bonds resulting from the deoxygenation process of *WS* under secondary reactions, e.g., Diels–Alder and repolymerization and increase the rate of carbonization [52]. To assess the impact of plastics on the co-pyrolysis process, it is necessary to consider several factors in advance. Firstly, it should be noted that in pyrolysis products of plastics, light olefins and styrene are capable of engaging in secondary reactions; however, this does not rule out the possibility of the participation of other olefins with lower reactivity. In general, as the number of carbons in olefins increases, their reactivity decreases clearly [53, 54]. Another aspect to take into account is the higher thermal stability of PE compared to PP, which leads to lower production of light olefin in the pyrolysis of PE under similar conditions. As a result, the reactivity of pyrolysis products of PE is lower than that of PP, a finding that has been confirmed by experiments. Moreover, the main pyrolysis product of PS is styrene, which has a considerable ability to participate in secondary reactions. Styrene possesses a double bond attached to the phenyl group, which, along with another double bond in the phenyl group, can form a cis-butadiene that is available for Diels–Alder reactions. The significant involvement of styrene in the secondary reactions during the co-pyrolysis process is demonstrated by the obtained results of the reactor and TG. Since the activity of styrene is much higher than light olefins and due to its higher molecular than light olefins, it spends more residence time in the reactor, as a result, as can be seen, PS is more effective than polyolefins and creates more new structures. The aromatic structures created along the charcoal surfaces, in addition to increasing the of the charcoal, lead to the creation of new porosities. Furthermore, the new polyaromatic structures that are formed on the pores of *WS* particles can increase the surface area and porosity, which can be seen in the results. The strong peak of double bonds and aromatics in the region of 1440 cm^{-1} confirms the formation of special polyaromatic structures on the surface of *WS* particles, which can only be seen in samples including plastic, and the FTIR graph of *WS* particles did not show this peak or it is very weak. The polyaromatic structures created on the surface of particles lead to a decrease in *WS* degradation rate, and hence, as can be seen especially in the TG diagrams of samples with PP and PS, at a temperature lower than 700 ℃, the remaining charcoal from co-pyrolysis was higher than the *WS* pyrolysis. The results of the reactor pyrolysis process also confirm the TG results and considering that the samples experience a lower heating rate, and the pyrolysis process was slower; therefore, the remaining charcoal from the co-pyrolysis process showed a better quality than the pyrolysis of *WS*.

Conclusions

In this work, the effect of plastic wastes including PE, PP, and PS on the production process of activated carbon using walnut shell was studied using a fixed-bed reactor by single-stage and two-stage methods. In the following, using the TG instrument, the *WS* carbonization was evaluated along with the plastic wastes. The results indicated that during the pyrolysis, the melted plastic surrounded the *WS* particles, acted like an insulator and somewhat reduced the heat that reached *WS* particles. Furthermore, some of the pyrolysis products of plastics that have high reactivity, e.g., styrene and light olefins reacted with *WS* degrading structure, which was full of radicals and double bonds, and created new structures. Due to the lower heating rate of *WS* particles, in addition to the reaction with the pyrolysis products of plastics and the intensification of secondary reactions, the newly created structures on *WS* charcoal, as seen in FTIR diagrams, were of polyaromatic type. The results indicated that the use of plastics has led to an increase in the surface area and *TPV* during the activation process. Furthermore, the lower degradation temperature of PS and also the high activity of styrene compared to other pyrolysis products have led to the production of activated carbons with more surface area and *TPV* compared to polyolefins. Overall, the use of PS can be regarded as a viable choice for enhancing both the quality and quantity of activated carbon production. SEM and FTIR results also showed that activated carbons can be prepared with different physical properties using single-stage and two-stage methods as well as different plastics. The use of plastics, in addition to improving the efficiency of the activation process, their pyrolysis products can provide the total energy required for the preparation of activated carbon. It should be noted that the plastic wastes used for this method must be free of minerals. Furthermore, using other plastics such as PET with a structure close to biomass can bring interesting results.

Acknowledgements The research leading to these results has also received funding from the Fund for Scientific Research Flanders (FWO) and innovation program/ERC grant agreement no.818607 (OPTIMA). This work was also performed in the framework of the Catalisti cluster SBO project WATCH (HBC.2019.0001 "Plastic waste to chemicals") and **PREFER** (The Plastics Refinery: No More Waste) with the financial support of VLAIO (Flemish Agency for Innovation and Entrepreneurship).

Author contributions HB helped in methodology, software, validation, and writing—review & editing; MRR contributed to conceptualization, software, and writing—original draft; ST, BG and ZI helped in software, writing—original draft; HMS contributed to methodology and validation; KMVG done methodology, validation, writing—review & editing, and supervision; MNH performed conceptualization, writing—original draft, writing—review & editing; MSA-A contributed to conceptualization, software, and writing—original draft.

References

1. Bernal V, Giraldo L, Moreno-Piraján JC. Thermodynamic study of triclosan adsorption from aqueous solutions on activated carbon: modelling of experimental adsorption isotherm and calorimetry data. J Therm Anal Calorim. 2020;139:913–21.
2. Tabak A, Sevimli K, Kaya M, Çağlar B. Preparation and characterization of a novel activated carbon component via chemical activation of tea woody stem. J Therm Anal Calorim. 2019;138:3885–95.
3. Menya E, Olupot P, Storz H, Lubwama M, Kiros Y, John M. Effect of alkaline pretreatment on the thermal behavior and chemical properties of rice husk varieties in relation to activated carbon production. J Therm Anal Calorim. 2020;139:1681–91.
4. Zhou X-M, Liu Y-F. Study on the preparation of high adsorption activated carbon material and its application as phase change energy storage carrier material. J Therm Anal Calorim. 2022. https://doi.org/10.1007/s10973-021-11122-5.
5. Li Y, Lin Y, Xu Z, Wang B, Zhu T. Oxidation mechanisms of H2S by oxygen and oxygen-containing functional groups on activated carbon. Fuel Process Technol. 2019;189:110–9.
6. Al-Musawi TJ, McKay G, Kadhim A, Joybari MM, Balarak D. Activated carbon prepared from hazelnut shell waste and magnetized by Fe3O4 nanoparticles for highly efficient adsorption of fluoride. Biomass Convers Biorefinery. 2022. https://doi.org/10.1007/s13399-022-02593-z.
7. Abbaci F, Nait-Merzoug A, Guellati O, Harat A, El Haskouri J, Delhalle J, et al. Bio/KOH ratio effect on activated biochar and their dye based wastewater depollution. J Anal Appl Pyrol. 2022;162:105452.
8. Stano G, Di Nisio A, Lanzolla AM, Ragolia M, Percoco G. Fused filament fabrication of commercial conductive filaments: experimental study on the process parameters aimed at the minimization, repeatability and thermal characterization of electrical resistance. Int J Adv Manuf Technol. 2020;111(9):2971–86.
9. Zhong L, Zhang Y, Wang T, Ji Y, Norris P, Pan W-P. Optimized methods for preparing activated carbon from rock asphalt using orthogonal experimental design. J Therm Anal Calorim. 2019;136:1989–99.
10. Ismail IS, Singh G, Smith P, Kim S, Yang J-H, Joseph S, et al. Oxygen functionalized porous activated biocarbons with high surface area derived from grape marc for enhanced capture of CO_2 at elevated-pressure. Carbon. 2020;160:113–24. https://doi.org/10.1016/j.carbon.2020.01.008.
11. Liu X, Zuo S, Cui N, Wang S. Investigation of ammonia/steam activation for the scalable production of high-surface area nitrogen-containing activated carbons. Carbon. 2022;191:581–92. https://doi.org/10.1016/j.carbon.2022.02.014.
12. Heidarinejad Z, Dehghani MH, Heidari M, Javedan G, Ali I, Sillanpää M. Methods for preparation and activation of activated carbon—a review. Environ Chem Lett. 2020;18(2):393–415.
13. Bazan A, Nowicki P, Półrolniczak P, Pietrzak R. Thermal analysis of activated carbon obtained from residue after supercritical extraction of hops. J Therm Anal Calorim. 2016;125:1199–204.
14. Gao Y, Yue Q, Gao B, Li A. Insight into activated carbon from different kinds of chemical activating agents—a review. Sci Total Environ. 2020;746:141094.
15. Shawabkeh RA, Aslam Z, Hussien IA. Thermochemical treatment of fly ash for synthesis of mesoporous activated carbon. J Therm Anal Calorim. 2015;122:1191–201.
16. Enterría M, Martín-Jimeno FJ, Suárez-García F, Paredes JI, Pereira MFR, Martins JI, et al. Effect of nanostructure on the supercapacitor performance of activated carbon xerogels obtained from hydrothermally carbonized glucose-graphene oxide hybrids.

Carbon. 2016;105:474–83. https://doi.org/10.1016/j.carbon.2016.04.071.
17. Oishi S, Amano Y, Aikawa M, Machida M. Adsorption of Pb(II) ion on mesoporous activated carbon prepared by $ZnCl_2$ activation. Carbon. 2012;50(3):1445. https://doi.org/10.1016/j.carbon.2011.11.023.
18. Giraldo L, Moreno-Piraján JC. CO_2 adsorption on activated carbon prepared from mangosteen peel: study by adsorption calorimetry. J Therm Anal Calorim. 2018;133:337–54.
19. de la Torre-Miranda N, Reilly L, Eloy P, Poleunis C, Hermans S. Thiol functionalized activated carbon for gold thiosulfate recovery, an analysis of the interactions between gold and sulfur functions. Carbon. 2023;204:254–67. https://doi.org/10.1016/j.carbon.2022.12.061.
20. Serafin J, Dziejarski B, Cruz Junior OF, Sreńscek-Nazzal J. Design of highly microporous activated carbons based on walnut shell biomass for H_2 and CO_2 storage. Carbon. 2023;201:633–47. https://doi.org/10.1016/j.carbon.2022.09.013.
21. Hassan MF, Sabri MA, Fazal H, Hafeez A, Shezad N, Hussain M. Recent trends in activated carbon fibers production from various precursors and applications—a comparative review. J Anal Appl Pyrol. 2020;145:104715.
22. Abdul Khalil H, Firoozian P, Jawaid M, Akil H, Hassan A. Preparation of activated carbon filled epoxy nanocomposites: morphological and thermal properties. J Therm Anal Calorim. 2013;113:623–31.
23. Abbas-Abadi MS. The effect of process and structural parameters on the stability, thermo-mechanical and thermal degradation of polymers with hydrocarbon skeleton containing PE, PP, PS, PVC, NR, PBR and SBR. J Therm Anal Calorim. 2021;143(4):2867–82. https://doi.org/10.1007/s10973-020-09344-0.
24. Salas-Enríquez BG, Torres-Huerta AM, Conde-Barajas E, Domínguez-Crespo MA, Díaz-García L, Negrete-Rodríguez MDLLX. Activated carbon production from the Guadua amplexifolia using a combination of physical and chemical activation. J Therm Anal Calorim. 2016;124:1383–98.
25. Pamphile N, Xuejiao L, Guangwei Y, Yin W. Synthesis of a novel core-shell-structure activated carbon material and its application in sulfamethoxazole adsorption. J Hazard Mater. 2019;368:602–12.
26. Amorós-Pérez A, Cano-Casanova L, Ouzzine M, Rufete-Beneite M, Romero-Anaya AJ, Lillo-Ródenas MÁ, et al. Spherical activated carbons with high mechanical strength directly prepared from selected spherical seeds. Materials. 2018;11(5):770.
27. Arantes HT, Machado MA, Santoro MC, Freitas JC, Ronconi CM, Ligiero CB, et al. Effect of activated biochar as a low-cost catalyst on the quality of catalytic intermediate co-pyrolysis oil from waste polystyrene and green coconut pericarp. Fuel Process Technol. 2023;240:107539.
28. Tazibet S, Velasco L, Lodewyckx P, Abou M'Hamed D, Boucheffa Y. Systematic study of the role played by $ZnCl_2$ during the carbonization of a chemically activated carbon by TG–MS and DSC. J Therm Anal Calorim. 2018;134:1395–404.
29. Heidari A, Khaki E, Younesi H, Lu HR. Evaluation of fast and slow pyrolysis methods for bio-oil and activated carbon production from eucalyptus wastes using a life cycle assessment approach. J Clean Prod. 2019;241:118394.
30. Abbas-Abadi MS, Van Geem KM, Alvarez J, Lopez G. The pyrolysis study of polybutadiene rubber under different structural and process parameters: comparison with polyvinyl chloride degradation. J Therm Anal Calorim. 2022;147(2):1237–49. https://doi.org/10.1007/s10973-020-10431-5.
31. Abbas-Abadi MS, Van Geem KM, Fathi M, Bazgir H, Ghadiri M. The pyrolysis of oak with polyethylene, polypropylene and polystyrene using fixed bed and stirred reactors and TGA instrument. Energy. 2021;232:121085.
32. Ryu HW, Kim DH, Jae J, Lam SS, Park ED, Park Y-K. Recent advances in catalytic co-pyrolysis of biomass and plastic waste for the production of petroleum-like hydrocarbons. Biores Technol. 2020;310:123473.
33. Abbas-Abadi MS, Jalali A, Rostami MR, Haghighi MN, Farhadi A. The atmospheric, vacuum and pressurized pyrolysis of used bleaching soils along with polymeric wastes to reach the valuable and economical fuels. J Clean Prod. 2020;255:120328. https://doi.org/10.1016/j.jclepro.2020.120328.
34. Seifali Abbas-Abadi M, Nekoomanesh HM. The consideration of different effective zeolite based catalysts and heating rate on the pyrolysis of Styrene Butadiene Rubber (SBR) in a stirred reactor. Energy Fuels. 2017;31(11):12358–63.
35. Bech N, Jensen PA, Dam-Johansen K. Determining the elemental composition of fuels by bomb calorimetry and the inverse correlation of HHV with elemental composition. Biomass Bioenerg. 2009;33(3):534–7.
36. Quek A, Balasubramanian R. Liquefaction of waste tires by pyrolysis for oil and chemicals—a review. J Anal Appl Pyrol. 2013;101:1–16.
37. Gao Y, Zheng B, Wu G, Ma F, Liu C. Effect of the Si/Al ratio on the performance of hierarchical ZSM-5 zeolites for methanol aromatization. RSC Adv. 2016;6(87):83581–8.
38. Önal E, Uzun BB, Pütün AE. Bio-oil production via co-pyrolysis of almond shell as biomass and high density polyethylene. Energy Convers Manage. 2014;78:704–10.
39. Muniandy L, Adam F, Mohamed AR, Ng E-P. The synthesis and characterization of high purity mixed microporous/mesoporous activated carbon from rice husk using chemical activation with NaOH and KOH. Microporous Mesoporous Mater. 2014;197:316–23.
40. Shagali AA, Hu S, Wang Y, Li H, Wang Y, Su S, et al. Comparative study on one-step pyrolysis activation of walnut shells to biochar at different heating rates. Energy Rep. 2021;7:388–96.
41. Bedia J, Peñas-Garzón M, Gómez-Avilés A, Rodriguez JJ, Belver C. Review on activated carbons by chemical activation with $FeCl_3$. C. 2020;6(2):21.
42. Alfattani R, Shah MA, Siddiqui MIH, Ali MA, Alnaser IA. Biochar characterization produced from walnut shell biomass through slow pyrolysis: sustainable for soil amendment and an alternate bio-fuel. Energies. 2021;15(1):1.
43. Abbas-Abadi MS, Haghighi MN, Yeganeh H, Bozorgi B. The effect of melt flow index, melt flow rate, and particle size on the thermal degradation of commercial high density polyethylene powder. J Therm Anal Calorim. 2013;114(3):1333–9.
44. Brebu M, Ucar S, Vasile C, Yanik J. Co-pyrolysis of pine cone with synthetic polymers. Fuel. 2010;89(8):1911–8.
45. Abbas-Abadi MS, Haghighi MN, Yeganeh H. Effect of the melt flow index and melt flow rate on the thermal degradation kinetics of commercial polyolefins. J Appl Polym Sci. 2012;126(5):1739–45.
46. Ding Y, Ezekoye OA, Lu S, Wang C, Zhou R. Comparative pyrolysis behaviors and reaction mechanisms of hardwood and softwood. Energy Convers Manage. 2017;132:102–9.
47. Greenhalf C, Nowakowski D, Harms A, Titiloye J, Bridgwater A. A comparative study of straw, perennial grasses and hardwoods in terms of fast pyrolysis products. Fuel. 2013;108:216–30.
48. Burhenne L, Messmer J, Aicher T, Laborie M-P. The effect of the biomass components lignin, cellulose and hemicellulose on TGA and fixed bed pyrolysis. J Anal Appl Pyrol. 2013;101:177–84.
49. Han B, Chen Y, Wu Y, Hua D, Chen Z, Feng W, et al. Co-pyrolysis behaviors and kinetics of plastics–biomass blends through thermogravimetric analysis. J Therm Anal Calorim. 2014;115(1):227–35.
50. Ahmed MB, Johir MAH, Zhou JL, Ngo HH, Nghiem LD, Richardson C, et al. Activated carbon preparation from biomass feedstock:

clean production and carbon dioxide adsorption. J Clean Prod. 2019;225:405–13.
51. Chen W, Gong M, Li K, Xia M, Chen Z, Xiao H, et al. Insight into KOH activation mechanism during biomass pyrolysis: chemical reactions between O-containing groups and KOH. Appl Energy. 2020;278:115730.
52. Abbas-Abadi MS, Zayoud A, Kusenberg M, Roosen M, Vermeire F, Yazdani P, et al. Thermochemical recycling of end-of-life and virgin HDPE: a pilot-scale study. J Anal Appl Pyrol. 2022;166:105614.
53. Abbas-Abadi MS, Ureel Y, Eschenbacher A, Vermeire FH, Varghese RJ, Oenema J, et al. Challenges and opportunities of light olefin production via thermal and catalytic pyrolysis of end-of-life polyolefins: towards full recyclability. Progr Energy Combust Sci. 2023;96:101046. https://doi.org/10.1016/j.pecs.2022.101046.
54. Abbas-Abadi MS, Kusenberg M, Zayoud A, Roosen M, Vermeire F, Madanikashani S, et al. Thermal pyrolysis of waste versus virgin polyolefin feedstocks: the role of pressure, temperature and waste composition. Waste Manage. 2023;165:108–18. https://doi.org/10.1016/j.wasman.2023.04.029.